Prell, W. L., Niitsuma, N., et al., 1991
Proceedings of the Ocean Drilling Program, Scientific Results, Vol. 117

30. INTERSTITIAL WATER CHEMISTRY, LEG 117: CONTRASTS WITH THE PERU MARGIN[1]

T. F. Pedersen[2] and G. B. Shimmield[3]

ABSTRACT

Interstitial water analyses made at 12 sites during Leg 117 are used to define the nature of diagenetic reactions in organic-rich sediments on the Owen Ridge and Oman Margin. Minor variations in chloride concentration profiles are ascribed to past changes in bottom water salinity at two mid-depth margin sites and to upward migration of low salinity water at another. There is no evidence for subsurface brine movement, unlike the case on the Peru Margin. Dolomitization is widespread and accounts for the depletions of magnesium observed in pore waters at variable depths at nearly all sites. The mineral occurs both as disseminated euhedral limpid crystals and, in at least one location, in massive stringers. Formation of the latter is suggested to reflect precipitation during sea level transgressions when the sedimentation rate was low, but when productivity was high. Authigenic carbonate fluorapatite is also widespread, the phosphorus being derived from the breakdown of organic matter. Sulfate is quantitatively depleted at depth at most locations but the rate of depletion is markedly less than that observed on the Peru Margin where sedimentation is also similarly influenced by high rates of upwelling. The reason for this contrast is not clear and merits further investigation.

INTRODUCTION

The Arabian Sea is one of the most productive regions in the world's oceans as a consequence of monsoon-driven upwelling (Qasim, 1982; Nair et al., 1989). The resulting high-settling flux of organic matter is primarily responsible for the relatively high concentrations of marine organic carbon found in sediments on the Oman Margin and, to a lesser extent, on the Owen Ridge (Fig. 1). The deposited organic detritus fuels a series of microbially-mediated diagenetic reactions which are manifest in the sediments by the precipitation of authigenic reaction products, and in the interstitial waters by depletion of oxidants, particularly sulfate, and the addition of dissolved metabolites. Interstitial water samples were collected at all sites drilled during Leg 117 and a series of analyses was performed on board in an effort to define the nature and extent of such chemical diagenesis in the three regionally contrasting depositional environments (the Indus Fan, Owen Ridge, and the Oman Margin) studied during the leg.

In addition to diagenesis, a number of other factors influence the chemistry of pore waters in the Arabian Sea. Sluggish intermediate-depth circulation and a pronounced settling flux of organic matter conspire to produce a widespread and severe oxygen minimum in the northern Arabian Sea (Wyrtki, 1971) between depths of about 200 and 1500 m. Thus, oxygen concentrations are extremely low in the bottom waters which bathe sediments on the Oman Margin. Presumably, the high organic carbon flux and the deficiency of oxygen in the water column should be reflected in the pore waters by the rapid consumption of sulfate; however, as discussed below, this is not the case. Major ion distributions in pore waters are also affected by variations in time and space of the salinity of bottom water masses. On the Oman Margin, the magnitude of such effects depends on the relative proportions of highly saline Red Sea and Persian Gulf outflow waters present at each location. Such hydrographic variations may be recorded by chloride (e.g., McDuff, 1985) and, to a lesser extent, salinity profiles. The influence of buried evaporites or subsurface dense brines on pore water chemistry is minor on the margin, unlike the situation encountered off Peru during Leg 112 (Suess, von Huene, et al., 1988); however, at least one site has been influenced by the presumably advective addition of fresher water from a distal location.

In this chapter we discuss the distributions of Cl^-, S, Ca^{2+}, Mg^{2+}, titration alkalinity, SO_4^{2-}, PO_4^{3-}, NH_4^+ and SiO_2 in pore waters collected from twelve drilling sites in the northwest Arabian Sea. Given the large number of descriptions of pore water chemistry published to date in DSDP and ODP proceedings, we shall avoid dwelling on previously well-described phenomena and will focus instead on several unique aspects of the data, in particular unexpectedly low rates of sulfate reduction, and dolomite formation. Only brief accounts of controls on the distributions of parameters judged to exhibit previously observed and well-documented behavior are offered.

METHODS

Samples were collected aboard the *JOIDES Resolution* by expressing pore fluids in a Manheim-type stainless steel squeezer, without applying precautions for the pressure or temperature-of-squeezing artifacts which have been described by Murray et al. (1980), Mangelsdorf et al. (1969), Bischoff et al. (1970), and Fanning and Pilson (1971). We do not feel that such artifacts have significantly compromised the quality of the data presented in this report. Standard ODP shipboard analytical methods were employed for all analyses reported here (Prell, Niitsuma, et al., 1989, p. 28–29) as follows: chloride—Knudsen microtitration, with $AgNO_3$ added with a Metrohm Dosimat titrator; SO_4^{2-}—ion chromatography; Ca^{2+}—colorimetric titration following Tsunogai et al. (1988); Mg^{2+}—determined as the difference between the total alkaline earths measured by colorimetric titration and the Ca^{2+} concentration; SiO_2, NH_4^+, and PO_4^{3-}—spectrophotometry, following Gieskes and Peretsman (1986); titration alkalinity—potentiometric (Gran) titration (Gieskes and Rogers, 1973) using a Metrohm autotitrator controlled by a Hewlett-Packard microcomputer. Salinity was estimated using a Reichert optical refractometer. The relative concentration of dissolved organic carbon (Gelbstoffe) was estimated at some sites by measuring the absorbance at 243.7 nm.

At some sites on the Oman Margin (particularly 723), high concentrations of H_2S interfered with the spectrophotometric

[1] Prell, W. L., Niitsuma, N., et al., 1991. *Proc. ODP, Sci. Results,* 117: College Station, TX (Ocean Drilling Program).
[2] Department of Oceanography, University of British Columbia, Vancouver, B.C. V6T 1W5, Canada.
[3] Grant Institute of Geology, University of Edinburgh, West Mains Road, Edinburgh EH9 3JW, United Kingdom.

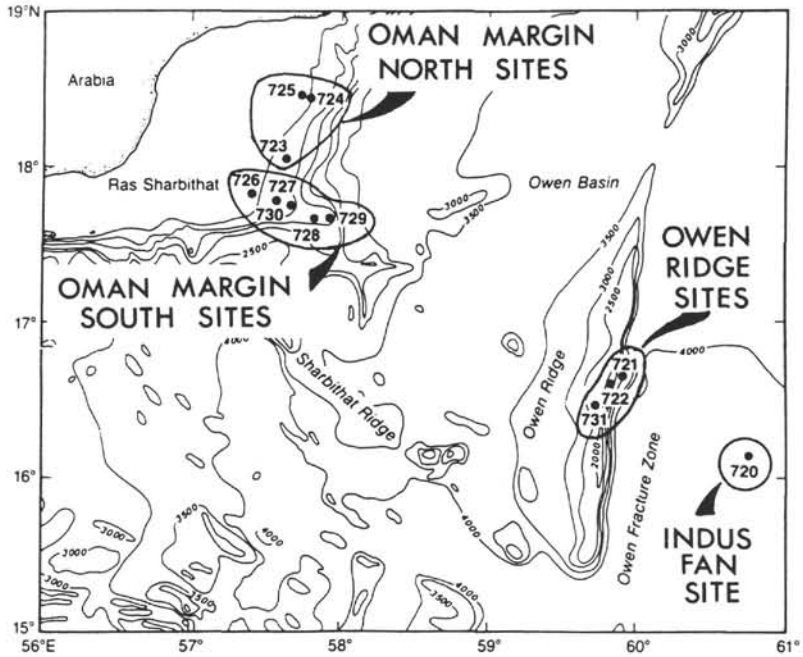

Figure 1. Location of the Arabian Sea sites drilled during Leg 117. For convenience of discussion, the sites have arbitrarily been grouped into the clusters shown.

determination of phosphate by causing turbidity in the colorimetric solutions, probably because of the precipitation of antimonyl sulfide during reagent addition. We circumvented this problem in samples from Hole 723C and at subsequent sites by bubbling wet N_2 through the samples to strip the H_2S prior to analysis.

The results of all measurements are listed in Table 1.

LITHOLOGIC SUMMARY

Holes were drilled during Leg 117 in three regionally distinct areas (Fig. 1): the distal Indus Fan (Site 720); the Owen Ridge (Sites 721, 722, 731), and the Oman Margin (Sites 723–730). Briefly, the Indus Fan sediments at Site 720 consist of turbiditic clastic deposits intercalated with pelagic nannofossil ooze. Organic carbon contents range widely between 0.03% and 3.7%, with most samples containing <1%. At the Owen Ridge sites foraminifer-bearing to foraminifer-nannofossil ooze-chalks of Holocene to late Miocene age overlie early late Miocene siliceous-bearing nannofossil to diatomaceous nannofossil chalk and middle Miocene nannofossil chalk. These pelagic deposits are underlain by early Miocene silt and mud turbidites. The ridge sediments are generally rich in organic matter, with C_{org} concentrations averaging ~1.2% ± 0.9% in the pelagic sections. The underlying turbidites typically contain <0.2% C_{org}.

Lithologies on the Oman Margin vary from site to site (see Prell, Niitsuma, et al., 1989). At Site 723 (808 m water depth) the deposits consist of marly nannofossil ooze with a variable terrigenous content. Dolomitic limestone and finely laminated siliceous and marly ooze occur as minor components below about 240 mbsf. A calcareous silty clay facies comprises the entire section cored at Site 724 (593 m water depth); at the shallow Site 725 (312 m water depth), organic- and opal-rich clayey silt alternates with nonlaminated nannofossil ooze and calcitic silty clay. Holocene to late Miocene silty clay and clayey silt alternate with nannofossil/foraminifer ooze in the upper 130 m cored at Site 726 (331 m water depth). These deposits overlie Eocene(?) shallow water limestones and dolomites. Calcitic marly nannofossil ooze to calcitic marly calcareous ooze characterizes the entire section cored at Site 727 at mid-depth (915 m) on the margin. The lower slope basin drilled at Site 728 (1428 m depth) hosts mainly marly nannofossil ooze. Poor recovery at Site 729 obviates further discussion of this location. Drilling at Site 730 (1066 m depth) penetrated a thin interval of Quaternary marly calcareous ooze unconformably overlying late Miocene to middle Miocene marly nannofossil ooze and diatomaceous silty clays. Early Miocene(?) calcareous marly chalks containing calcareous turbidites were recovered in the lower half of the 400 m deep hole.

Organic carbon contents vary widely both between sites on the margin and as a function of sedimentary facies. Highest concentrations, on the order of 7 wt. %, occur in sporadic intervals at Sites 723 and 724; on average C_{org} contents in margin sediments are 2%–3%. Organic carbon accumulation rates, calculated using shipboard C_{org} measurements, and bulk accumulation rates determined from biostratigraphic age datums and measured bulk densities (Prell, Niitsuma, et al., 1989) tend to be high (Table 2), ranging up to a maximum of 900 mg cm^{-2} kyr^{-1} at Site 723. The mean accumulation rate, however, is on the order of 200 ± 150 mg cm^{-2} kyr^{-1} over much of the margin. This average value is similar to that observed on the highly productive Peru Margin, roughly 250 (range 10-600) mg cm^{-2} kyr^{-1}, calculated from data published in Suess, von Huene, et al. (1988).

RESULTS AND DISCUSSION

For convenience in presentation and discussion of the data, we have clustered the pore water profiles into three groups based on geographical separation: the Owen Ridge sites (721, 722, and 731), Oman Margin North (723,724, and 725), and Oman Margin South (726, 727, 728, and 730). Site 720 (Indus Fan) is discussed separately where appropriate; Site 729 is not included in the discussion as noted above. Note that where more than one hole was drilled at a given site, the data have been combined, strictly on the basis of sub-bottom depth without adjustment for possible offsets. In most cases this poses no problem and the oceanographic consistency of the stacked profiles attests to the

Table 1. Leg 117 interstitial water data.[a]

Sample	Depth (mbsf)	pH	Alkalinity (mmol/L)	S (g/kg)	Mg^{2+} (mmol/L)	Ca^{2+} (mmol/L)	Cl^- (mmol/L)	SO_4^{2-} (mmol/L)	PO_4^{3-} (μmol/L)	NH_4^+ (mmol/L)	SiO_2 (μmol/L)	Mg/Ca	DOC (a.u.)[b]
Site 720													
1H-4, 145–150	5.95	7.54	5.08	34.3	50.28	7.85	554	21.4	9.6	0.58	626	6.41	
3H-3, 145–150	23.45	7.80	6.73	33.0	41.19	4.73	558	8.5	13.9	1.18	162	8.71	
7X-1, 145–150	59.05	7.68	5.58	31.8	31.40	5.91	544	0.0	1.9	2.01	218	5.31	
11X-2, 145–150	99.35	7.55	3.88	32.2	31.22	7.29	546	0.0	1.5	2.79	391	4.28	
16X-1, 145–150	146.15	7.79	3.12	31.7	30.88	6.35	543	0.0	1.6	3.09	233	4.86	
19X-2, 140–150	176.60	8.00	4.09	31.0	29.98	6.55	545	0.0	1.0	2.47	116	4.58	
24X-1, 140–150	223.40	7.97		31.0	31.07	6.89	548	0.0	0.6	2.43	121	4.51	
30X-1, 145–150	284.25	7.63	5.68	30.6	28.93	6.81	543	0.0	3.8	3.12	1014	4.25	
40X-1, 140–150	377.30	7.96	2.50	31.8	26.32	9.36	547	0.0	0.2	2.19	80	2.88	
Holes 721A,B													
A 1H-6, 145–150	8.95	7.38	5.47	34.3	49.25	7.61	556	20.9	8.7	0.60	855	6.47	
B 3H-5, 145–150	26.55	7.66	6.99	34.2	45.35	7.01	557	15.0	8.6	1.03	846	6.47	
A 3H-6, 145–150	28.45			33.7	43.16	6.75	552	12.0	10.3	1.26	914	6.39	
B 6H-4, 145–150	54.05	7.74	9.02	33.5	37.42	5.94	558	6.8	12.4	1.66	1100	6.30	
A 6H-6, 145–150	57.45	7.88		32.0	36.29	6.20	554	6.1	30.7	1.84	1075	5.85	
B 9H-4, 145–150	82.35	7.42	10.72	32.2	32.77	5.93	556	2.8	12.0	2.07	1083	5.53	
A 9H-6, 145–150	85.75	7.76	11.56	32.2	31.81	6.10	554	2.0	13.2	1.99	1117	5.21	
I 12I-1, 000–001	100.00	8.02	9.75	32.3	33.39	6.08	556	0.0	2.2	2.19	1024	5.49	
B 12X-1, 145–150	106.65	7.61	10.55	32.2	30.54	6.42	560	0.5	12.9	2.37	1075	4.76	
I 15I-1, 000–001	129.00	7.84	10.57	31.7	30.37	6.92	559	0.0	23.2	2.48	948	4.39	
B 15X-5, 145–150	141.55	7.28	9.58	32.2	29.26	7.54	562	0.0	9.7	2.32	948	3.88	
B 18X-5, 145–150	170.65	7.28	8.87	32.2	28.18	7.99	557	0.2	6.3	2.51	889	3.53	
B 22X-5, 145–150	209.45	7.31	7.77	32.0	27.44	8.89	564	0.0	4.9	2.34	745	3.09	
B 24X-2, 140–150	224.20	7.23	7.36	32.2	26.31	9.31	557	0.0	3.8	2.39	872	2.83	
B 27X-3, 145–150	254.25	7.26	5.90	32.2	26.26	9.44	557	0.0	2.6	2.14	770	2.78	
B 30X-2, 140–150	282.10	7.42	5.20	32.2	26.14	9.79	559	0.0	5.3	1.96	897	2.67	
B 33X-1, 140–150	309.80	7.41	4.34	32.2	26.58	9.67	563	0.0	3.6	1.91	762	2.75	
B 36X-1, 140–150	338.80	7.33	3.60	32.2	25.49	9.89	567	0.0	0.5	1.79	178	2.58	
B 40X-5, 140–150	383.30	7.78	2.59	32.2	26.13	10.83	567	0.0	0.4	1.07	280	2.41	
B 44X, 140–150	421.90	7.94	1.63	33.0	26.74	11.96	573	4.6	0.8	1.06	51	2.24	
Holes 722A,B													
A 1H-4, 145–150	5.95	7.48	5.00	33.0	49.90	8.22	549	23.0	7.2	0.51	678	6.07	
A 3H-4, 145–150	25.35	7.61	6.75	33.0	44.60	6.88	555	14.8	9.9	1.20	893	6.49	
A 6H-4, 145–150	54.15	7.73	8.05	32.5	37.00	6.10	554	8.1	8.8	1.82	104	6.07	
A 9H-4, 145–150	82.75	7.79	9.11	32.3	34.40	6.18	556	3.5	7.8	1.92	1032	5.56	
A 12X-4, 145–150	111.85	7.61	7.94	32.2	30.80	7.15	555	1.0	7.4	2.14	1042	4.31	
A 15X-5, 145–150	142.35	7.56	6.91	32.0	28.99	7.48	559	0.7	4.5	2.31	1012	3.88	
A 19X-4, 145–150	179.55	7.49	6.25	32.0	29.17	8.71	556	0.7	3.2	2.13	916	3.35	
A 22X-4, 145–150	208.65	7.33	5.63	31.8	27.86	9.55	558	1.0	2.7	2.15	1014	2.92	
A 27X-2, 140–145	253.90	7.32	4.91	32.3	27.31	10.10	562	0.0	2.4	2.08	1190	2.70	
B 27X-4, 140–150	252.40	7.67	4.85	31.8	27.14	10.14	563	0.0	2.0	1.93	1190	2.68	
I 30X-1, 000–001	275.60	7.35	4.02	34.4	39.42	11.47	566	1.0	2.3	1.59	846	3.44	
B 31X-4, 140–150	291.20	7.38	4.16	32.0	27.26	11.21	565	0.0	1.5	1.92	1257	2.43	
B 34X-2, 140–150	317.20	7.48	3.68	32.5	29.21	11.98	563	1.0	1.5	1.56	1161	2.44	
B 37X-5, 140–150	350.80	7.19	3.02	32.4	27.15	12.88	566	1.0	0.7	1.51	1208	2.11	
B 40X-2, 140–150	375.40	7.44	2.11	32.6	27.70	13.41	568	2.4	0.7	1.19	646	2.07	
B 43X-2, 140–150	404.30	7.49	1.49	32.8	28.00	13.58	570	2.4	0.0	1.21	167	2.06	
B 46X-5, 140–150	437.90	7.53	1.83	33.0	29.20	15.48	569	3.5	0.9	0.63	320	1.89	
B 49X-1, 140–150	463.80	7.58	1.81	32.0	28.17	15.58	548	3.9	0.3	0.61	226	1.81	
B 52X-5, 140–150	495.60	7.66	1.62	32.8	29.08	17.15	558	4.6	0.3	0.43	322	1.70	
B 58X-4, 140–150	552.10	7.63	1.69	33.0	28.94	18.69	562	3.5	0.4	0.41	361	1.55	
Holes 723A,C													
C 1H-2, 145–150	2.95	7.70	10.45		55.66	7.77		20.6	12.0	1.20	477	7.16	
A 1H-4, 145–150	5.95	7.65	7.42	36.0	54.15	8.58	568	23.2	9.5	1.22	423	6.31	
C 1H-5, 145–150	7.45	7.80	12.04		55.09	7.07		18.1	15.2	1.40	562	7.79	
C 2H-2, 145–150	10.75	7.80	12.71		52.99	6.88		16.6	10.8	1.56	703	7.70	
C 2H-5, 145–150	15.25	8.00	13.99		54.69	6.76		16.3	8.1	1.81	580	8.09	
C 3H-2, 145–150	20.45	8.10	17.35		51.25	6.56		11.8	6.9	2.04	625	7.81	
A 3H-4, 145–150	23.45	8.14	18.40	35.0	48.28	7.26	569	12.2	24.6	2.51	937	6.65	
C 3H-5, 145–150	24.95	8.10	20.66		44.67	6.01		6.1	6.7	2.13	770	7.43	
C 4H-2, 145–150	30.05	8.00	27.39		37.99	5.72		13.0	8.4	3.89	799	6.64	
C 4H-5, 145–150	34.55	7.70	29.68		37.12	5.56		8.5	8.3	5.80	838	6.68	
C 5H-2, 145–150	39.75	7.80	32.50		35.57	5.53		2.2	13.0	6.91	1030	6.43	
C 5H-5, 145–150	44.25	7.80	35.26		37.71	5.29		0.0	11.4	9.13	1004	7.13	
I 6I-1, 000–001	46.40	7.70	30.17		41.40	7.36		4.6	43.6	7.77	1110	5.58	
C 6H-2, 145–150	49.35	7.60	36.28		36.56	5.09		0.7	14.4	11.69	991	7.18	
A 6H-4, 145–150	52.35	7.38	40.60	34.2	35.26	5.17	559	0.0	19.9	12.17	991	6.82	
C 6H-5, 145–150	53.85	7.80	36.47		34.92	4.91		0.0	18.2	12.96	1082	7.11	
C 7H-3, 145–150	59.46	7.60	41.45		35.33	4.74		1.6	16.7	15.09	1030	7.45	
C 7H-6, 145–150	63.96	7.80	45.33		36.62	4.48		0.0	16.0	16.06	1053	8.17	
I 8I-1, 000–001	65.80	7.60	43.96		43.96	7.99		7.3	19.4	13.08	1077	5.50	

Table 1 (continued).

Sample	Depth (mbsf)	pH	Alkalinity (mmol/L)	S (g/kg)	Mg^{2+} (mmol/L)	Ca^{2+} (mmol/L)	Cl^- (mmol/L)	SO_4^{2-} (mmol/L)	PO_4^{3-} (μmol/L)	NH_4^+ (mmol/L)	SiO_2 (μmol/L)	Mg/Ca	DOC (a.u.)[b]
Holes 723A,C (Cont.)													
C 8H-2, 145–150	68.75	7.70	43.85		36.79	3.99		0.7	19.4	18.14	1082	9.22	
C 8H-5, 145–150	73.25	7.80	35.67		35.67	3.45		0.0	19.2	20.03	1077	10.34	
I 9I-1, 000–001	75.40	7.70	58.91		38.61	7.32		0.7	6.8	17.77	1230	5.27	
A 9H-4, 145–150	81.35	7.58	47.20	34.2	33.12	3.25	553	0.0	23.2	20.46	941	10.19	
A 13X-4, 140–150	120.05	7.49	73.90	35.4	33.09	4.04	540	0.0	37.4	28.29	1020	8.19	
A 17X-1, 145–150	154.25		76.30	35.0	28.65	2.66	534	0.0	29.5	35.25	1062	10.77	
A 20X-4, 145–150	187.75	7.26	82.40	35.4	25.98	3.00	534	0.0	27.7	37.04	1085	8.66	
A 23X-1, 145–150	212.25	7.96	88.50	35.2	22.82	1.77	532	0.0		37.84	1042	12.89	
A 26X-3, 145–150	244.25	7.51	91.60	35.5	22.60	2.76	529	0.6	32.5	39.62	1052	8.19	
A 29X-6, 145–150	277.65	7.55	97.70	35.0	20.65	2.07	531	1.1	31.3	41.00	1211	9.98	
A 32X-5, 145–150	304.95	7.47	97.80	35.2	18.92	2.39	529	0.4	34.6	40.00	1144	7.65	
A 36X-5, 145–150	333.54	7.21	106.80	36.0	19.09	2.74	533	1.6	32.3	40.40	1196	6.97	
A 39X-5, 145–150	362.45	7.06	93.90	36.0	17.35	2.92	533	1.9	29.8	40.40	1211	5.94	
A 42X-1, 140–150	385.40	7.81	106.70	36.0	16.67	4.08	527	2.2	27.4	37.00	1401	4.09	
Holes 724A,B,C													
C 1H-1, 145–150	1.45	7.60	5.00	35.9	55.49	10.29	565	26.3	3.2	0.50	330	5.30	
A 1H-3, 145–150	4.45	8.10	5.40	35.0	51.24	8.59	570	19.4	3.8	1.02	512	5.98	
C 2H-4, 145–150	8.75	8.00	6.40	36.5	55.32	8.74	564	23.5	4.5	0.65	395	6.33	
A 3H-4, 145–150	21.85	7.67	5.74	35.0	45.96	9.03	572	13.9	7.3	1.35	466	5.09	
C 3H-4, 145–150	18.15	8.20	6.90	36.3	51.64	9.16	574	22.1	5.3	0.76	404	5.64	
C 4H-4, 145–150	27.65	8.20	8.68	36.2	45.38	9.78	575	13.9	3.7	1.02	483	4.64	
C 5H-4, 145–150	37.15	8.30	12.70	35.0	39.64	8.84	578	6.6	1.7	1.70	675	4.48	
B 6X-3, 145–150	49.45		13.02	34.0	32.35	7.47	578	0.9	2.7	2.35	963	4.33	
B 9X-4, 145–150	79.95	7.81	13.91	33.0	25.70	6.57	561	0.7	7.1	7.61	1148	3.91	
B 12X-5, 145–150	110.45	7.70	19.66	32.5	25.32	6.00	555	1.1	8.5	12.33	998	4.22	
B 16X-4, 145–150	147.65	7.70	21.68	32.5	23.31	4.75	557	1.8	3.5	15.04	984	4.91	
B 19X-4, 145–150	176.65	7.70	28.45	32.5	20.79	4.72	554	0.7	4.5	18.37	1017	4.40	
B 23X-3, 145–150	213.85	7.10	27.18	33.5	18.74	4.55	555	1.5	7.7	19.29	1073	4.12	
B 25X-4, 145–150	234.65	7.00	28.75	33.8	17.30	4.80	558	1.8	7.7	19.49	1138	3.60	
Holes 725A,B,C													
A 1H-2, 145–150	2.95	7.70	3.67	35.6	54.32	10.63	576	27.2	2.8	0.65	183	5.11	
B 5X-1, 145–150	37.65	8.15	4.77	35.6	46.11	13.03	583	21.3	1.6	1.40	310	3.54	
C 3H-4, 145–150	24.55	8.37	4.66	35.5	46.95	11.96	584	21.5	1.2	1.02	248	3.93	
C 6X-2, 145–150	50.45	8.29	10.56	35.4	43.60	12.00	587	15.5	6.4	3.10	914	3.63	
C 9X-3, 145–150	80.55	8.05	17.31	36.0	41.90	13.49	592	13.5	3.6	4.53	1272	3.11	
C 12X-3, 145–150	109.35	7.96	27.16	34.8	31.12	8.75	583	0.8	5.1	9.15	1195	3.56	
C 15X-4, 145–150	139.75	8.32	32.20	34.2	27.41	7.34	569	1.1	2.0	16.47	1262	3.73	
C 17X-5, 145–150	160.65	7.95	33.93	34.2	22.13	5.39	565	0.8	2.0	21.34	1135	4.11	
Hole 726A													
A 1H-4, 145–150	5.95	7.93	4.41	35.8	53.31	11.15	574	26.5	2.1	0.07	147	4.78	
A 3H-4, 145–150	22.25	7.76	3.04	36.3	50.96	13.42	582	26.4	0.7	0.22	251	3.80	
I 4H-7, 000–001	34.80	7.80	2.69	36.3	50.71	13.67	588	26.1	1.1	0.27	461	3.71	
A 6H-4, 145–150	50.65	7.78	5.43	36.3	45.89	15.80	588	22.6	7.0	0.58	885	2.90	
A 9X-2, 145–150	76.15	7.89	5.63	36.3	45.80	17.00	595	22.6	8.1	0.69	964	2.69	
A 13X-4, 145–150	117.75	7.55	3.42	36.3	45.90	18.72	593	25.5	2.6	0.21	427	2.45	
Hole 727A													
A 1H-4, 145–150	5.95	7.99	6.34	35.8	53.49	9.94	569	24.6	5.5	0.50	285	5.38	
A 3H-4, 145–150	24.85	8.19	10.96	34.9	47.81	7.75	569	15.2	3.0	0.64	603	6.17	
A 4I-6, 000–001	35.90	8.26	18.26	34.4	36.09	6.91	569	1.6	1.1	0.82	925	5.22	
A 6H-4, 145–150	53.25	7.86	21.48	33.8	29.89	6.27	566	0.0	2.3	5.59	990	4.77	
A 9H-4, 145–150	82.05	7.48	27.60	33.0	30.76	5.56	558	1.6	11.6	12.71	940	5.53	
A 11I-1, 000–001	95.40	7.42	39.57	34.6	32.94	6.96	558	0.0	19.1	16.08	953	4.73	
A 12X-4, 145–150	110.95	7.51	35.34	33.6	32.68	5.47	557	1.3	15.0	18.57	923	5.97	
A 15X-5, 145–150	141.35	7.58	44.07	34.4	32.33	5.58	554	1.0	18.6	23.29	942	5.79	
A 18X-3, 145–150	167.45	7.30	44.56	34.2	33.66	6.00	554	2.4	21.6	24.08	904	5.61	
Holes 728A,B													
A 1H-4, 145–150	5.95	7.50	3.83	35.0	52.36	10.27	558	25.4	6.1	0.22	293	5.10	0.141
B 2H-4, 145–150	7.15	7.30	3.73	35.5	52.32	10.23	559	24.0	6.2	0.17	305	5.11	0.113
A 3H-4, 145–150	25.05	7.90	4.13	35.4	52.14	9.54	565	24.4	6.2	0.40	394	5.47	0.294
B 4H-4, 145–150	26.05	7.70	4.78	35.8	56.05	9.84	556	26.1	5.3			5.70	0.260
B 7I-1, 000–001	48.60	8.20	9.19	34.7	48.05	9.02	570	16.3	4.0	2.52	775	5.33	2.059
A 6H-4, 145–150	53.45	8.10	9.35	35.0	46.45	8.15	568	12.7	10.6	1.89	929	5.70	0.987
B 7H-4, 145–150	54.55	7.70	10.15	35.5	43.54	8.20	569	12.7	7.2	1.51	995	5.31	0.898
A 9H-4, 145–150	82.05	8.00	13.63	32.6	33.91	6.65	565	0.0	8.2	3.43	1046	5.10	1.328
B 10X-4, 145–150	83.25	7.20	17.49	33.2	33.30	6.60	565	0.0	11.4	1.19	1038	5.05	1.535
B 13I-1, 000–001	106.10	7.40	18.19	32.8	31.90	8.95	565	0.5	18.2	3.36	1016	3.56	1.225
A 12X-2, 145–150	107.85	8.00	15.56	32.5	32.81	8.04	565	0.0	6.4	4.14	1127	4.08	1.360
A 15X-4, 145–150	139.85	7.70	13.30	32.2	28.10	8.06	565	0.0	12.0	4.89	1098	3.49	1.172

Table 1 (continued).

Sample	Depth (mbsf)	pH	Alkalinity (mmol/L)	S (g/kg)	Mg^{2+} (mmol/L)	Ca^{2+} (mmol/L)	Cl^- (mmol/L)	SO_4^{2-} (mmol/L)	PO_4^{3-} (μmol/L)	NH_4^+ (mmol/L)	SiO_2 (μmol/L)	Mg/Ca	DOC (a.u.)[b]
Holes 728A,B (Cont.)													
B 18I-1, 000-001	154.40	7.70	16.11	32.4	28.53	9.62	560	0.0	19.7	4.54	1081	2.97	1.168
A 18X-4, 145-150	168.75	7.60	12.57	32.3	28.34	8.54	564	1.3	10.9	5.21	1053	3.32	0.980
A 21X-4, 145-150	197.75	7.20	12.02	32.2	25.14	9.59	564	0.0	12.6	5.75	1225	3.12	0.891
A 24X-3, 145-150	225.25	7.20	10.58	32.1	24.35	9.99	563	0.0	9.8	5.84	1233	2.44	0.795
B 26I-1, 000-001	231.80	7.60	11.91	32.4	23.83	10.98	560	0.0	8.4	6.01	1143	2.17	0.735
A 27X-4, 145-150	255.75	7.20	8.99	32.0	23.09	10.37	563	0.0	12.7	5.90	1235	2.23	0.685
A 30X-4, 145-150	284.75	7.30	7.75	32.0	22.35	11.35	562	0.0	9.9	5.75	1153	1.97	0.557
A 33X-4, 145-150	313.75	7.40	6.18	32.2	22.86	11.40	561	0.3	8.8	5.71	1129	2.01	0.470
A 36X-4, 145-150	342.75	7.40	5.57	32.0	22.35	12.09	560	0.0	9.3	5.69	1227	1.84	0.396
Hole 729A													
A 1R-2, 145-150	2.95	7.50	3.74	35.8	52.63	10.02	562	24.6	3.0	0.13	198	5.25	
A 3R-4, 145-150	18.65	7.50	2.34	35.9	57.84	10.27	562	24.3	1.5	0.14	350	6.63	
Hole 730A													
A 1H-4, 145-150	5.95	7.64	3.48	35.2	52.94	10.65	563	26.1	2.5	0.13	170	4.97	0.075
A 3H-4, 145-150	23.75	7.11	2.84	35.2	51.33	10.98	564	26.1	2.3	0.16	576	4.67	0.110
A 6X-4, 145-150	52.25	7.23	3.71	35.0	49.72	12.04	568	23.1	2.4	0.22	917	4.13	0.223
A 9X-4, 145-150	81.15	7.47	5.29	34.3	41.66	12.39	565	14.9	3.5	0.35	1065	3.36	0.532
A 12X-4, 145-150	110.15	7.40	6.33	33.6	35.89	12.28	566	7.6	2.5	0.74	1129	2.92	0.726
A 15X-4, 145-150	139.15	7.68	6.75	32.6	32.72	12.98	562	3.7	1.7	1.01	1097	2.52	0.793
A 18X-4, 145-150	168.15	7.45	5.34	32.6	30.29	13.11	564	2.2	1.6	1.22	1252	2.31	0.731
A 21X-4, 145-150	197.15	7.59	5.17	32.4	28.41	14.19	564	0.4	3.5	1.48	1103	2.00	0.680
A 24X-4, 145-150	226.15	7.61	4.34	32.4	28.26	14.58	564	0.4	3.2	1.60	1008	1.94	0.467
A 27X-2, 140-150	252.10	7.39	4.10	32.3	27.58	15.02	564	0.0	4.6	1.84	998	1.84	0.406
A 29X-4, 140-150	274.50	7.42	3.73	32.3	27.84	15.08	557	0.0	3.0	2.03	1141	1.85	0.340
A 33X-3, 140-150	331.60	7.42	3.27	32.2	28.07	15.41	564	0.0	2.0	2.29	850	1.82	0.305
A 37X-2, 140-150	348.80	7.16	3.12	32.2	26.99	16.81	567	0.0	1.0	2.64	800	1.61	0.292
A 39X-1, 140-150	366.60	7.15	2.76	32.2	26.93	16.79	569	0.0	1.0	2.88	733	1.60	0.223
A 42X-2, 140-150	397.10	7.48	1.92	32.2	26.68	17.04	566	0.0	0.7	2.49	669	1.57	0.236
Holes 731A,B,C													
A 1H-4, 145-150	5.95	7.65	5.60	34.2	51.15	8.06	559	22.2	9.8	0.16	722	6.34	0.243
A 3H-4, 145-150	25.25	7.41	7.83	34.2	49.55	6.96	562	16.1	11.9	0.96	815	7.12	0.623
A 6H-4, 145-150	53.75	7.60	8.77	33.2	41.50	6.51	563	9.3	12.0	1.61	982	6.37	0.885
A 7I-6, 000-001	64.80	7.65	6.80	33.9	44.37	7.21	565	12.1	1.4	1.28	788	6.15	0.429
A 9X-4, 145-150	82.65	7.64	9.06	32.5	37.99	6.68	560	6.0	8.7	1.79	918	5.69	0.908
A 12X-4, 145-150	111.65	7.58	7.68	32.3	34.92	7.84	559	4.2	5.8	1.84	957	4.45	0.605
A 15X-4, 145-150	140.65	7.44	6.33	32.2	33.23	8.66	561	3.9	4.7	1.66	963	3.84	0.453
A 18X-4, 145-150	169.65	7.45	5.33	32.2	31.45	9.09	562	3.5	4.2	1.63	1114	3.46	0.378
A 21X-4, 145-150	198.75	7.56	3.41	32.2	30.27	9.71	559	3.2	3.2	1.46	1223	3.12	0.300
A 24X-4, 145-150	227.85	7.30	4.52	32.1	29.19	10.47	559	2.0	1.9	1.38	1126	2.79	0.256
A 27X-4, 145-150	256.85	7.45	3.44	32.0	28.26	10.69	557	2.0	0.7	1.25	1219	2.64	0.172
A 30X-4, 145-150	285.85	7.58	2.39	32.1	27.71	10.84	555	1.7	0.2	1.18	698	2.56	0.120
A 33X-2, 145-150	311.85	7.63	1.67	32.1	27.31	12.11	560	0.5	0.1	1.01	417	2.25	0.186
A 37X-1, 140-150	347.20	7.67	2.24	32.0	27.22	12.28	561	0.0	0.2	0.50	310	2.22	0.121
A 40X-2, 140-150	374.80	7.84	2.25	32.3	28.66	13.86	564	2.0	0.1	0.17	317	2.07	0.179
A 43X-4, 140-150	405.30	7.87	2.16	32.1	27.22	14.03	565	0.2	0.1	0.35	230	1.94	0.143
B 3X-1, 140-150	429.50	7.84	2.10	33.0	27.65	14.24	577	4.4	0.5	0.68	168	1.94	0.106
C 2R-2, 140-150	505.30	7.79	1.79	31.3	25.58	16.22	560	1.1	0.4	0.41	174	1.58	0.133
C 10R-1, 140-150	735.00	8.27	0.83	32.2	19.89	20.07	580	1.1	0.6	0.79	90	0.99	0.183
C 12R-1, 140-150	792.90	8.10	1.14	32.2	20.04	21.84	579	2.11	0.1	0.61	100	0.92	0.166
C 14R-1, 140-150	850.80	8.18	1.28	32.1	19.08	24.44	580	0.7	1.0	0.82	110	0.78	0.140
C 16R-2, 140-150	910.20	7.73	0.71	32.3	22.05	24.55	580	2.4	0.3	0.56	96	0.90	0.193
C 19R-2, 140-150	939.00			32.8	21.36	25.64	579	2.4	0.5	0.59	110	0.83	0.224
C 22R-3, 140-150	969.50	8.26	1.20	32.5	20.89	25.47	582	1.1	0.5	0.82	78	0.82	0.160
C 24R-3, 140-150	988.90		1.04	33.6	24.93	24.55	575	5.1	0.1	0.69	86	1.02	0.160

[a] Where more than one hole was drilled at a site, the data have been combined according to sub-bottom depth, assuming that the sediments were laterally homogeneous over the relatively large depth scales encountered. Sample names correspond to the standard ODP format. Note that *H* in the sample name indicates collection of the sediment with the Advanced Piston Corer, *X* designates use of the Extended Core Barrel drilling head, *R* indicates rotary drilling, and *I* indicates collection using the Barnes *in-situ* sampler.

[b] Dissolved organic carbon is reported in absorbance units (a.u.) and is a relative measure only.

validity of the assumption that the deposits are laterally homogeneous, at least within the coarse sampling resolution characteristic of ODP pore water collection. Results of measurements made on samples collected with the Barnes in situ sampler are included in Table 1. Some of the samples, particularly those from Site 723, were contaminated with drill water, however, and therefore have not been plotted.

Salinity and Chloride

At most locations, salinity decreases at depth (Table 1) independently of chloride as a direct consequence of sulfate reduction and extraction of Mg^{2+} from pore water. Relative to bottom water, the decreases range up to ~ 4 g kg^{-1}. At the Indus Fan Site 720, for example, lower salinity at depth (Table 1) can

be largely accounted for by the loss of most of the HCO_3^- which would have been produced as a consequence of the reduction of ~28 mmol L^{-1} of SO_4^{2-} (3 g kg^{-1} S), and about 25 mmol L^{-1} of Mg^{2+} (0.7 g kg^{-1} S). Presumably, the "missing" alkalinity and Mg^{2+} reflect precipitation of authigenic carbonate minerals, as discussed below. Similar considerations apply at the other sites, with the notable exception of Site 723 on the Oman Margin. At this location the salinity decreases to a minimum at about 50 mbsf (meters below seafloor) before increasing to about 36 below ~300 mbsf (Table 1). The deep increase is not accompanied by a commensurate chloride enrichment and therefore does not reflect uptake of water into clays or proximity to evaporites. Instead, we ascribe the deep S increase to the extremely high alkalinity observed at depth (described below); 100 mmol L^{-1} of HCO_3^- is equivalent to ~7 g kg^{-1} of salt, which more than compensates for the ~3.5 g kg^{-1} of lost sulfate and magnesium.

At Site 723, chloride decreases with depth, reaching a minimum value of 527 mmol L^{-1} (Fig. 2) at 385 mbsf. This distribution probably reflects dilution of the pore waters by upward diffusion and/or advection of fresher water. A similar but less pronounced decrease occurs at Site 727 (Fig. 2), which is located at a similar water depth some 50 km to the south. Distinct chloride maxima occur at Sites 724 and 725 between sub-bottom depths of 25 and 50 m, and 50 and 100 m, respectively (Fig. 2). The increase in concentration relative to bottom water (about 25 mmol L^{-1}) is considerably greater than the ~1% increase with depth commonly observed in the top 40 m at DSDP or ODP sites (McDuff, 1985). The latter distributions have been explained by McDuff (1985) as being a result of diffusion of salt through pore waters in response to glacial-interglacial changes in mean oceanic salinity. Such a mechanism cannot explain the distributions at the proximal northern Sites 724 and 725, however, because the chloride maxima occur at significantly different depths at the two locations (Fig. 2); if the distributions had been caused by downward diffusion from a saltier Pleistocene ocean, then the maxima would appear at the same depths because the sites have similar porosities and lithologies and diffusion would have acted in a like fashion at both locations. Plotting the two profiles on a common age scale (Fig. 3) offers an alternate, and somewhat speculative, explanation. The temporal coincidence of the Cl^- maxima suggests that more saline bottom water may have been buried with the sediments during the mid-Pleistocene at the two sites. The source of water of sufficient salinity to account for the maxima, giving due allowance for diffusion since the time of burial, is not clear, however.

Silicate

Two main factors control the dissolved silica distribution at the ridge and margin sites. First, dissolution of biogenic opal releases silica to solution. Where the sedimentary opal content is significant, pore water silica concentrations are high, in many cases reaching concentrations approximately at the solubility limit for opal (~1100 μmol L^{-1}; Hurd and Theyer, 1975). Second, the dissolved silica deficiency observed at depth on the Owen Ridge (Table 1) cannot simply reflect a paucity of opal in the turbidites below about 300 mbsf because the rate of sedimentation of the nannofossil oozes just above the turbidites is about half the effective rate of diffusion of dissolved SiO_2. Therefore, the low silica concentrations below 400 m depth must reflect precipitation. Indeed, both silica overgrowths on discoasters and replacement of discoaster calcite by SiO_2 are observed in the turbidites (Prell, Niitsuma, et al., 1989).

Sulfate and Alkalinity

Pronounced and essentially quantitative reduction of sulfate occurs at all sites drilled with the exception of the slowly accumulating silty clays and nannofossil oozes at Site 726. On the Owen Ridge, sulfate concentrations fall to very low or zero values by about 100 mbsf (Fig. 4); on the margin, sulfate is depleted at depths as shallow as 44 mbsf (Fig. 5). In general, the depth at which SO_4^{2-} is depleted is inversely related to the organic carbon accumulation rate as can be seen by comparing Figure 5 with Table 2. This relationship is a reflection of the

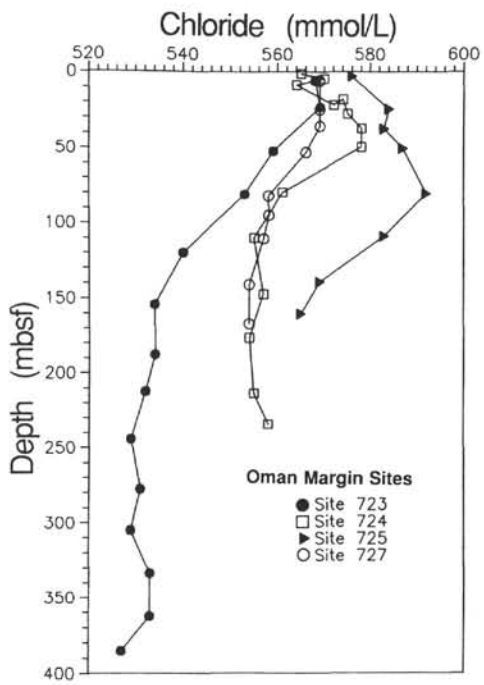

Figure 2. Interstitial chloride profiles at Sites 723, 724, 725, and 727 on the Oman Margin.

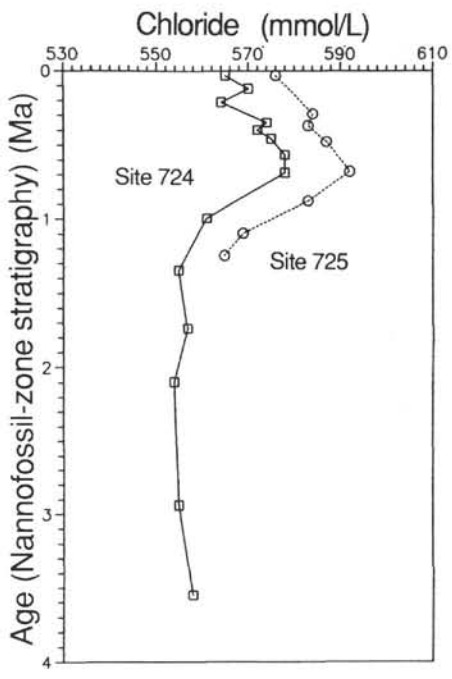

Figure 3. Chloride profiles at Sites 724 and 725 plotted on a common age scale.

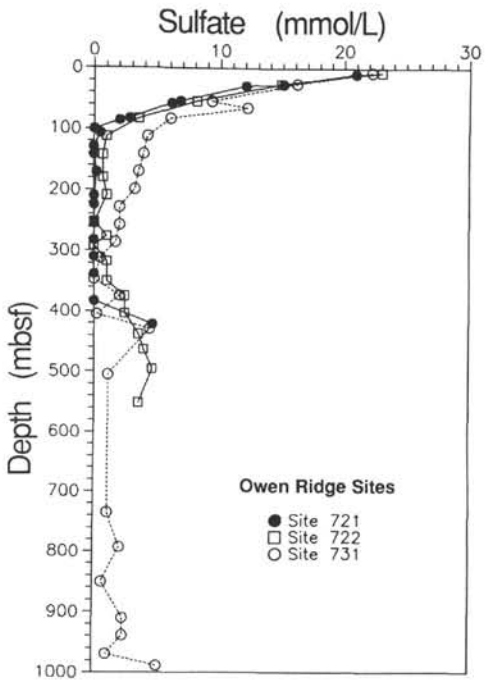

Figure 4. Interstitial sulfate profiles for Owen Ridge sites, Leg 117.

Table 2. Approximate organic carbon accumulation rates at Oman Margin drilling sites.

Site	[C_{org}] (wt.%)	Mean [C_{org}] (wt.%)	C_{org} accumulation (rate, mg cm^{-2} $k.y.^{-1}$)
723	0.71–6.83	3.2	340–900
724	0.32–7.32	3.0	90–370
725	0.22–4.16	2.5	40–200
726	0.43–4.79	2.5	29–115
727	0.80–4.96	2.5	200–400
728	~1.0–4.0	~2	~20–235
[a]730	0.92–3.4	2.3	~40–140

Note: Data compiled from Prell, Niitsuma, et al. (1989).
[a]Top 100 m only.

higher bacterial oxidant demand associated with faster accumulation of degradable organic matter; the latter, in turn, is often positively correlated with the bulk accumulation rate (Müller and Suess, 1979).

Titration alkalinity (predominantly HCO_3^-) is theoretically produced in the ratio 2:1 relative to sulfate when the latter is used as the terminal electron acceptor during the degradation of organic matter (e.g., Sholkovitz, 1973). Therefore, quantitative reduction of the 28 mmol L^{-1} of sulfate found in normal seawater should produce about 56 mmol L^{-1} of alkalinity, in the absence of other sources or precipitation reactions which remove carbonate species from solution. As can be seen by comparing Figures 6 and 7 with Figures 4 and 5, the alkalinity at all sites with the exception of 723 is less than would be predicted on the basis of the sulfate profiles. This deficiency is attributed to widespread precipitation of authigenic carbonate minerals as discussed below.

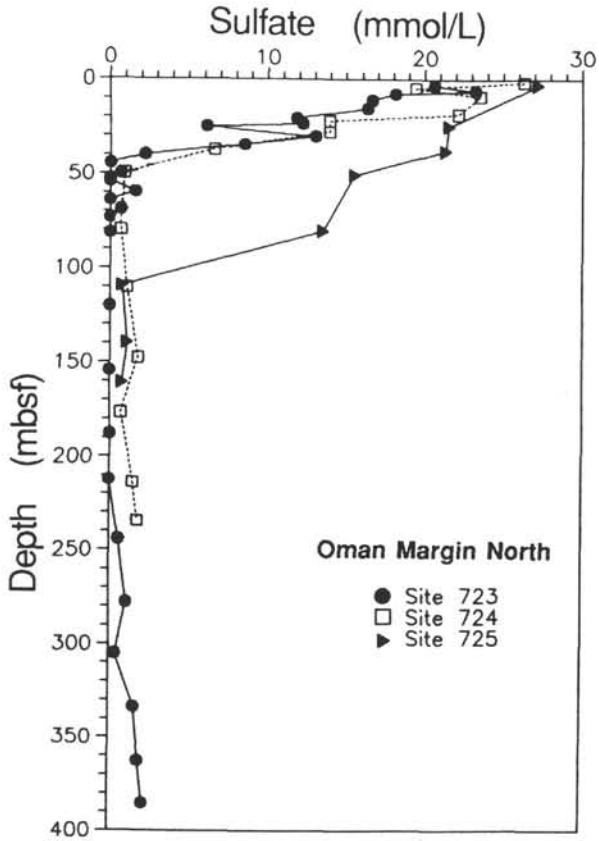

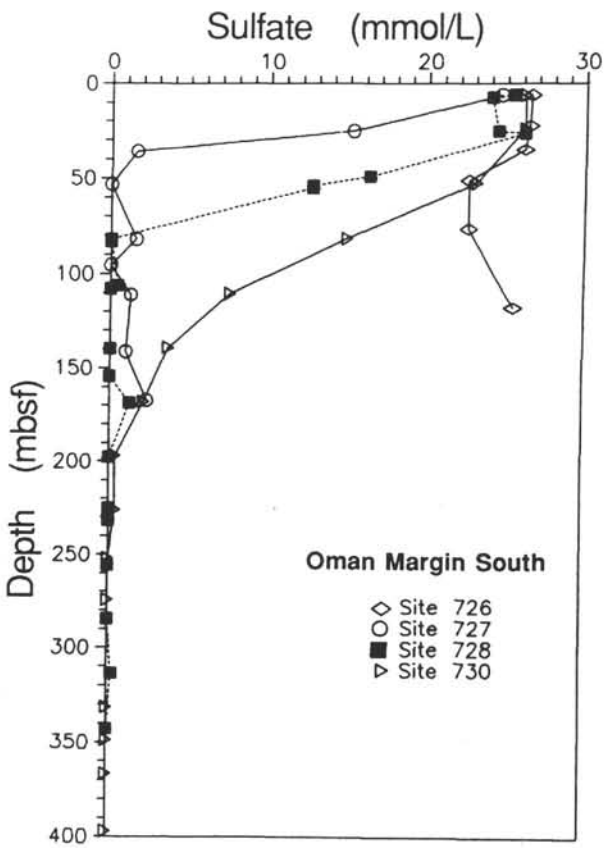

Figure 5. Interstitial sulfate profiles for Oman Margin sites, Leg 117.

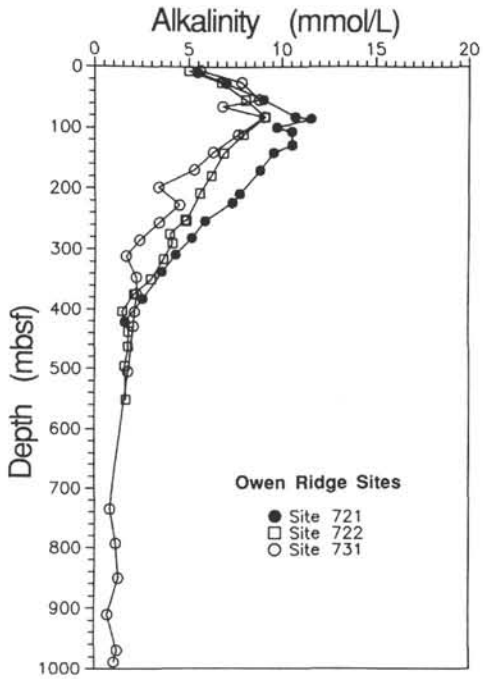

Figure 6. Titration alkalinity in interstitial waters at Owen Ridge sites, Leg 117.

The distributions of both alkalinity and sulfate at depth at Site 723 are unusual. The high resolution profile shown in Figure 5 indicates that the sulfate concentration falls to zero near 44 mbsf. However, significant concentrations of up to 2.2 mmol L^{-1} were measured in the lower 200 m of Hole 723A (Fig. 5); the gradual increase with depth between 240 and 400 mbsf suggests that sulfate is diffusing upward from a source below the base of the cored sequence. Bacterial reduction of the upward-diffusing sulfate may be occurring at almost any depth between 200 and 400 mbsf. It is not possible given the available resolution to pinpoint more precisely the zone or zones of reaction in the lower half of the hole. The titration alkalinities measured in 723A are among the highest ever observed during the history of deep-sea drilling, exceeding 100 mmol L^{-1} near the bottom of the hole (Fig. 7). These very high levels must reflect a source or sources of alkalinity other than that which can be produced by reduction of the total sulfate inventory of buried seawater. One source for the "excess" alkalinity must be the generation of ammonia and bicarbonate via methane-producing fermentation reactions, which increases titration alkalinity by producing HCO_3^- and hydroxyl, the latter in the reaction $NH_3 + H_2O = NH_4^+ + OH^-$. In Hole 723A, ammonium concentrations increase with depth by about 20 mmol L^{-1} in the zone between ~60 and 200 m depth (Table 1; Fig. 10) where no sulfate is present; this distribution most probably reflects production of ammonia during methanogenesis. Methane is abundant throughout this portion of the sediment column at the site (Prell, Niitsuma, et al., 1989). Between ~185 and 385 mbsf, where sulfate is present, alkalinity increases by ~20 mmol L^{-1} while ammonia increases only by about 3 mmol L^{-1}. Presumably, the maintenance of high alkalinity in this zone reflects the reduction of sulfate which is diffusing upward from a deep-seated source and continuing to pro-

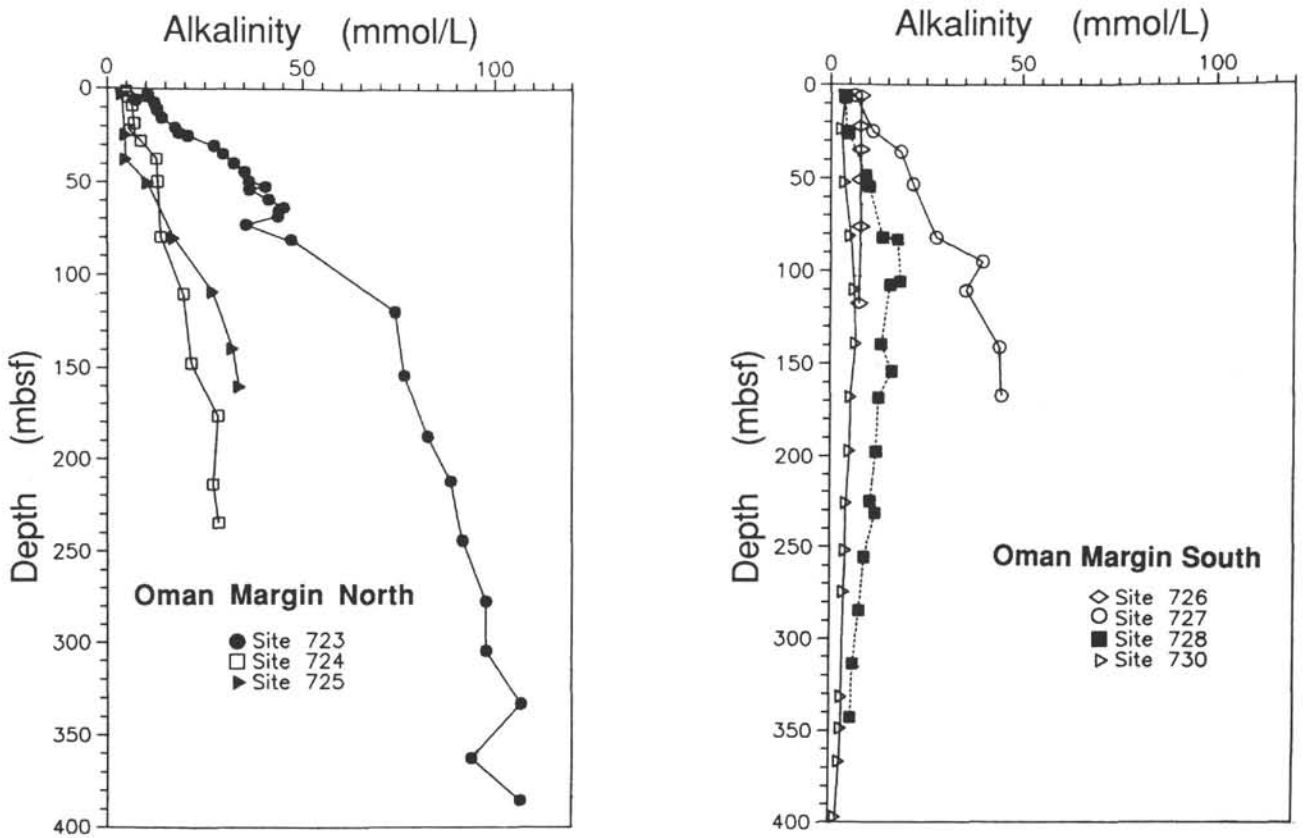

Figure 7. Titration alkalinity in interstitial waters at Oman Margin sites, Leg 117.

duce HCO_3^-. In addition, upward diffusion of carbonate could contribute to the observed distribution of alkalinity in the lowermost 200 m of the hole. Such phenomena were observed on the Peru Margin during Leg 112, where both chloride and sulfate profiles indicated that upward-diffusing brines were supplying sulfate to zones of reduction at depth in a number of holes (Suess, von Huene, et al., 1988). A major difference between the Peru Margin model and our observations here, however, is that the chloride concentration at Site 723 decreases with depth. We speculate that the only mechanism which can explain the observed trio of distributions (the chloride decrease, the deep alkalinity, and sulfate increases with depth) is diffusion related to an underlying fluid which is sulfate-enriched and chloride-depleted. Such a fluid could be produced by the percolation of relatively fresh groundwater through gypsum or anhydrite beds. The proximity of such deposits is unknown, however. If such a mechanism was active, one would expect calcium, in addition to sulfate, to be added to the percolating water. A small increase in the calcium concentration with depth is indeed observed in the lower 100 m of Hole 723A (Table 1), which tends to support our suggestion. Further support for the idea of upward migration of fluid at this site is furnished by downhole logging results, which indicate that the sediments at depth are undercompacted, probably as a consequence of pervasive upward or subhorizontal fluid flow (Prell, Niitsuma, et al., 1989, p. 360).

Calcium and Magnesium

The distributions of dissolved calcium and magnesium at the three Owen Ridge sites are essentially identical (Fig. 8). The downward concavity of the Ca^{2+} profile over the top 100 m and

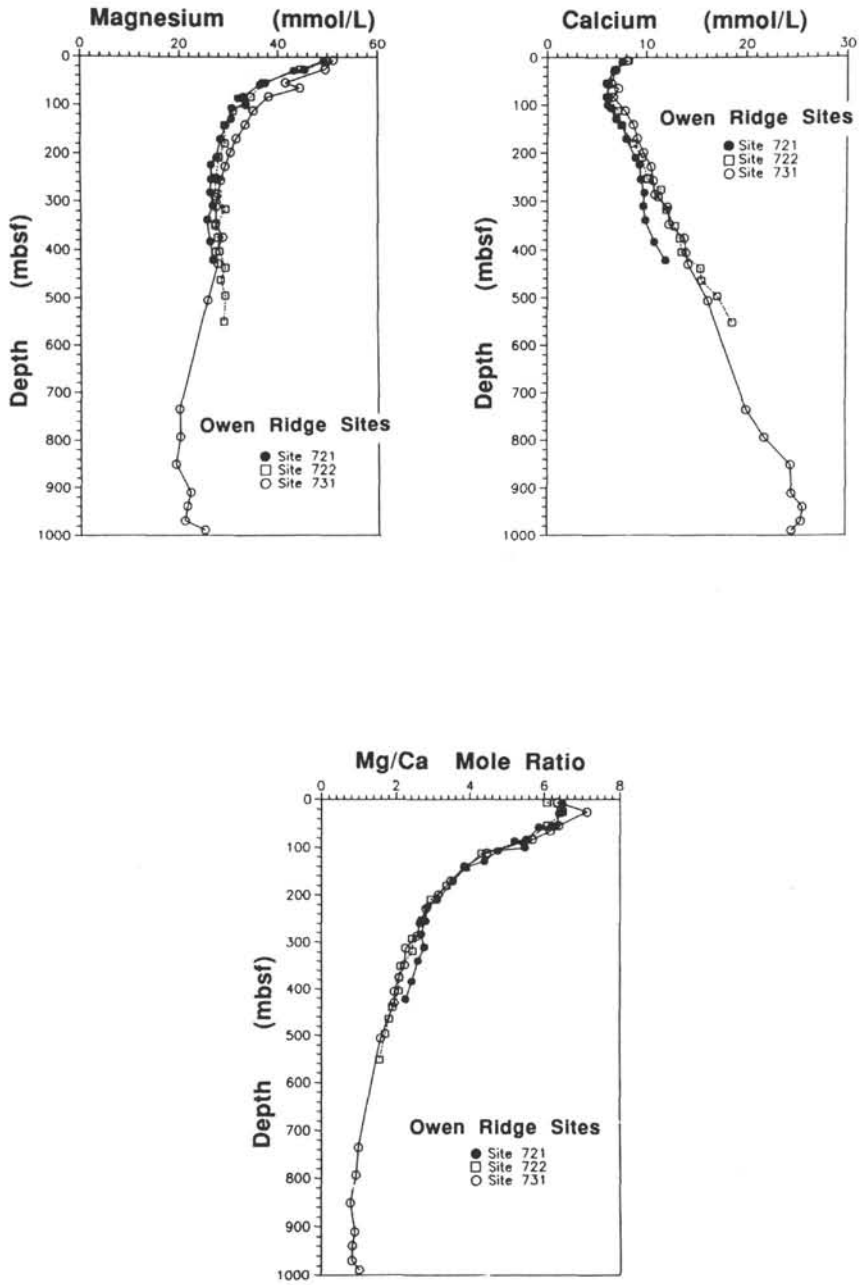

Figure 8. Calcium, magnesium, and Mg/Ca profiles in interstitial water at Owen Ridge sites, Leg 117.

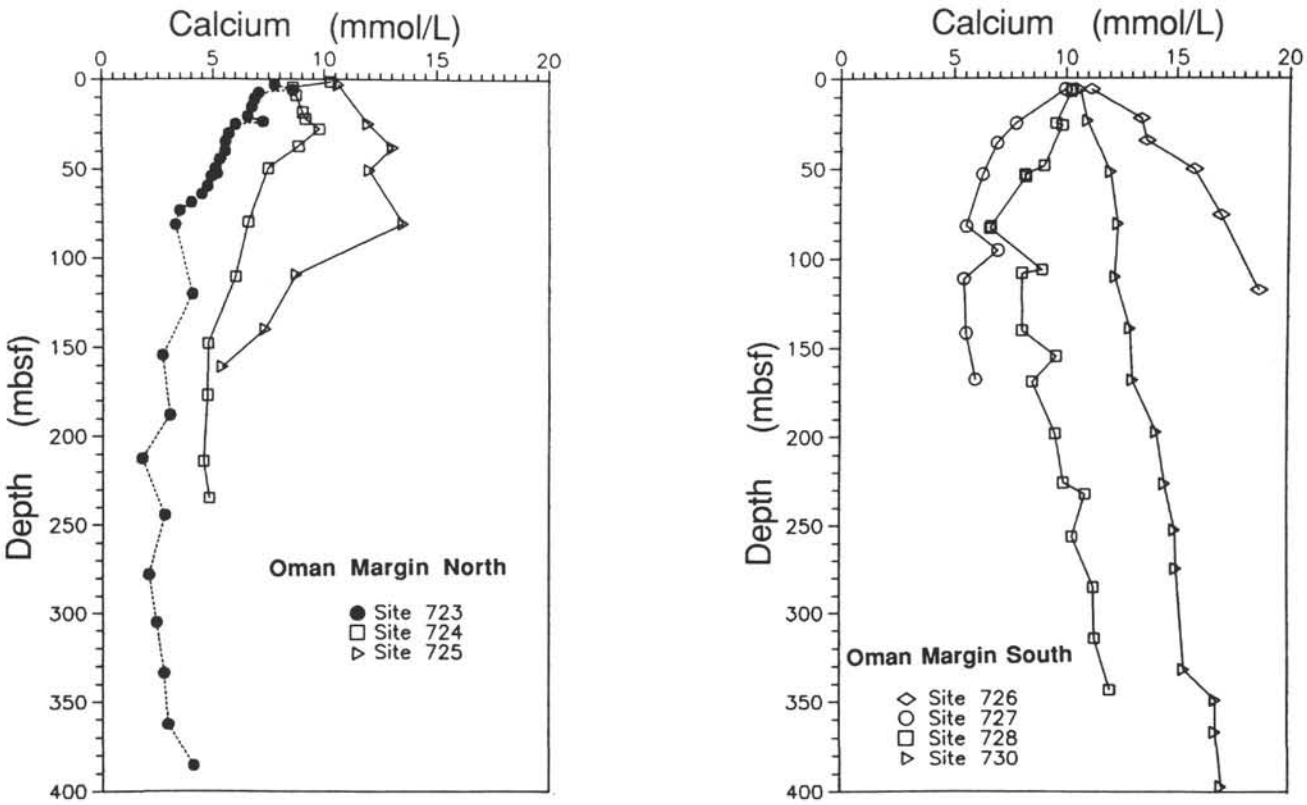

Figure 9. Calcium, magnesium, and Mg/Ca profiles in interstitial water at Oman Margin sites, Leg 117.

Mg^{2+} over the top 300 m indicates that both ions are removed from solution in these sections. Below 100 m, the calcium content increases approximately linearly to nearly 1 km sub-bottom depth, suggesting control by diffusion from a source near the bottom of the hole. Similar considerations apply to Mg^{2+} in the section between 400 and 1000 mbsf. The steady first-order decline in the Mg/Ca ratio over the 1000 m of section sampled on the ridge indicates that precipitation or alteration reactions consume substantially more magnesium than calcium from the pore solutions. These distributions are ascribed to precipitation of carbonate phases, including dolomite, as described below, and to alteration of volcanic ash and lithic fragments in the Miocene to late Oligocene(?) turbidites which comprise the lower two-thirds of the section (~350–1000 mbsf) in Hole 731C. Smear slide observations indicate that ash is a common minor constituent in the turbidites, ranging up to 10% by volume. Alteration of this material to magnesian smectite or possibly sepiolite may account for some of the observed Mg^{2+} depletion. Similarly, Ca^{2+} may be released to solution during the alteration of feldspars (and ash?) in the turbidites, particularly in the lowermost 150 m of the hole where Ca^{2+} concentrations are highest; indeed smear slide observations indicate that alteration of feldspars is a common phenomenon in the turbidite facies (S. Clemens, pers. comm.).

At most Oman Margin sites, as on the Owen Ridge, dissolved magnesium is significantly depleted at depth, unlike Ca^{2+}, which is depleted at some sites and enriched at others (Fig. 9). The depletion of both elements is particularly severe at Site 723, where extremely high alkalinities occur below depths of only ~50 mbsf. Presumably, precipitation of calcite is responsible for the increase in the Mg/Ca ratio seen in the top 15 m at this site. Immediately below this level, the magnesium concentration decreases quite markedly to ~37 mmol L^{-1} at 40 mbsf which we attribute to precipitation of authigenic dolomite. At other sites, both precipitation of dolomite and dolomitization of calcite may explain the ubiquitous magnesium depletions along with occasional calcium enrichments. Similar conclusions have been drawn to explain the comparable distributions of dissolved magnesium and calcium at Peru Margin drilling sites (Suess, von Huene, et al., 1988).

It is noteworthy that the changes observed in the Mg^{2+} and Ca^{2+} distributions reported here are typically most profound within the zone of sulfate reduction, which is still open to diffusional contact with overlying seawater, but well above any influence that the alteration of basaltic or mafic-type basement may have on pore water chemistry (commonly evinced by the concurrent depletion of magnesium and elevation of calcium (Sayles and Manheim, 1975; McDuff and Gieskes, 1976)).

Authigenic dolomite occurs in several forms on the Owen Ridge and the Oman Margin. At shallow depths (~10–100 mbsf), disseminated, euhedral, limpid rhombs were clearly observed in smear slides. No evidence of transport attrition was visible. At greater depths the quantity of euhedral dolomite typically increased, although the distribution was patchy in time and space. Finally, in the rapidly deposited and organic-rich sediments at Site 723, well-lithified stringers or beds of almost pure dolomite up to a meter thick were intersected and the mineralogy determined by X-ray diffractometry. Geophysical logging over the top 400 m at the site outlined nine "hard streaks" in total which are interpreted as being dolomite stringers (Prell, Niitsuma, et al., 1989, pp. 356–357).

Based on these observations and the pore water data, we propose a tentative model for the formation of dolomite on the Oman Margin. During sulfate reduction, alkalinity increases to a point where the solubility product of calcite is exceeded, fostering precipitation of $CaCO_3$ which increases the Mg/Ca ratio

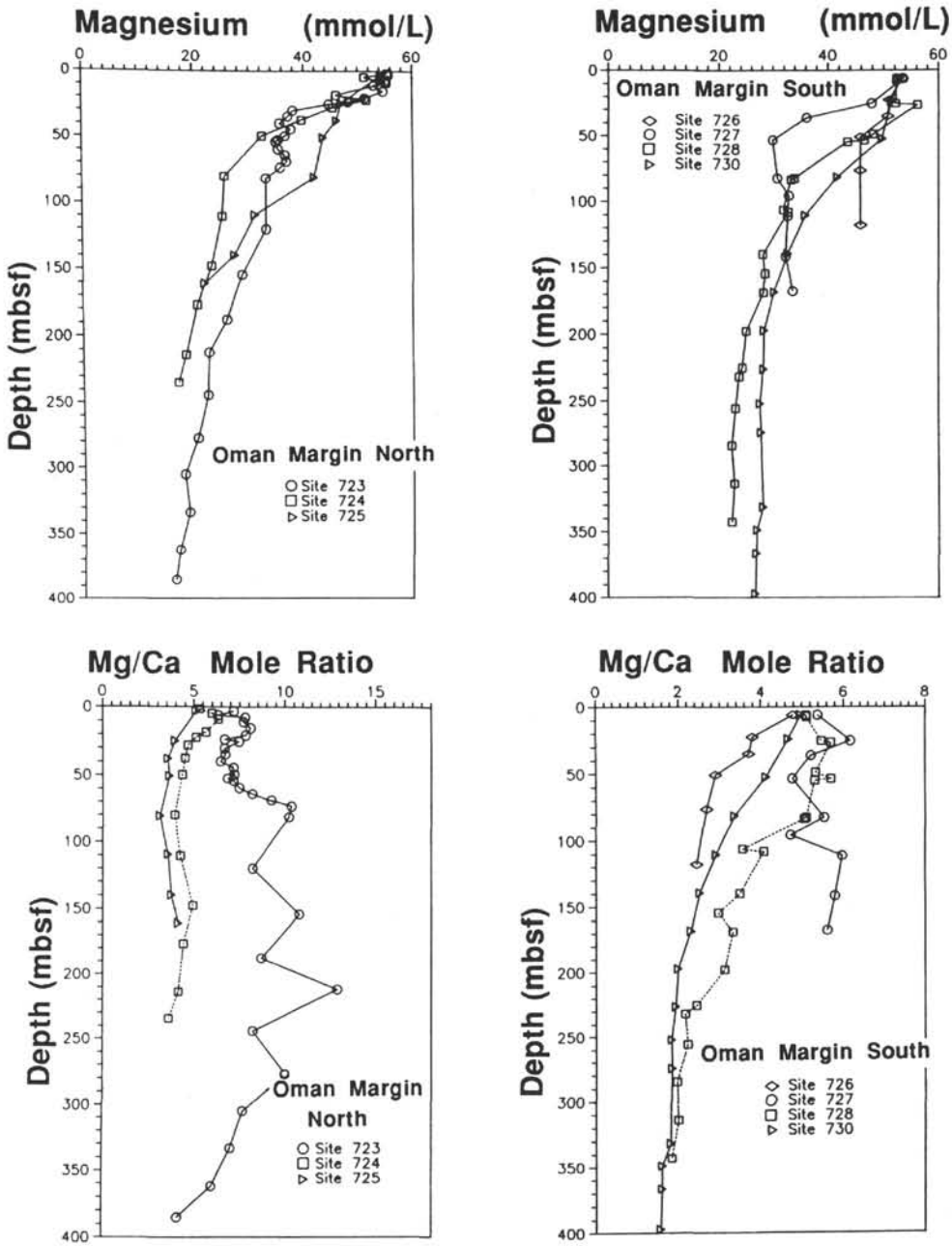

Figure 9 (continued).

(as seen in the upper 20 m of the high resolution records for Sites 723 and 724), making subsequent formation of dolomite chemically more favorable. Dolomite can precipitate via a number of pathways, including the following (Baker and Burns, 1985):

(1) $2CaCO_3 + Mg^{2+} = CaMg(CO_3)_2 + Ca^{2+}$ (replacement of aragonite or calcite);

(2) $Ca^{2+} + Mg^{2+} + 4HCO_3^- = CaMg(CO_3)_2 + 2CO_2 + 2H_2O$ (direct precipitation from solution); and

(3) $CaCO_3 + Mg^{2+} + 2HCO_3^- = CaMg(CO_3)_2 + CO_2 + H_2O$ (addition of magnesium without Ca^{2+} release).

As dolomite formation subsequently commences, the Mg^{2+} concentration and therefore the Mg/Ca ratio drop, as seen at most of the margin sites. Note that the Mg/Ca ratio in seawater is >5, the theoretical stability limit for dolomite vs. calcite precipitation. The occurrence of ratios lower than this at depth suggests that at some sites reaction (1) above may be applicable. This is not true for Site 723, however.

The dolomite layers at Site 723 range up to nearly a meter in thickness. It is clear that they could not have formed at any significant depth in the sediments because it is physically impossible for vertical diffusion to supply much magnesium (and/or calcium) to precipitation loci at depth in rapidly accumulating deposits. We suggest, therefore that the formation of the dolomite layers must have commenced when those horizons were near the sediment-water interface. Because reactions (2) and (3) above would be more likely to proceed when the HCO_3^- is high, a rapid accumulation of organic carbon, which would lead to

high alkalinity in interstitial waters, would facilitate dolomite formation. A slowed rate of sedimentation will also permit more Mg^{2+} to diffuse to the precipitation site from overlying seawater. Therefore, we suggest that the dolomite layers at Site 723 represent periods of high organic matter input coincident with episodes of reduced sedimentation. Such an association has been proposed previously to explain the distribution of dolomite in Holocene sediments off Baja California (Shimmield and Price, 1984). The depositional conditions required to support such a model are met at times of maximum transgression of sea level and lead to the formation of condensed sections (Haq et al., 1987). Deposition under an oxygen minimum would also be a positive influence in that low oxygen concentrations in bottom water would ensure that degradation of organic matter proceeds largely via sulfate reduction, which keeps the alkalinity high.

The ubiquity of dolomite formation on the Oman Margin and Owen Ridge suggests that the hypothesis of Baker and Kastner (1981), regarding the necessity for extensive sulfate depletion before dolomitization can commence, may not be universally applicable. It is clear from the pore water data that Mg^{2+} depletion relative to Ca^{2+} occurs well within the zone of sulfate occurrence. Formation of dolomite during early diagenesis is confirmed by smear slide observations of fresh, euhedral crystals of the mineral at shallow depths. Precipitation of dolomite was also noted to occur in the presence of copious concentrations of sulfate at Peru Margin sites during Leg 112 (Suess, von Huene, et al., 1988). Therefore, although the presence of sulfate or other large anions may indeed retard precipitation of dolomite from a suitable solution, we suggest that the primary requirement for dolomite formation in hemipelagic deposits is a high organic matter input coupled with a relatively low sediment accumulation rate. A similar model has been proposed to explain the widespread occurrence of authigenic dolomite on the Peru Margin (Suess, von Huene, et al., 1988).

Ammonia and Phosphorus

Ammonia concentrations range widely in Leg 117 pore waters, with extremely high concentrations being encountered at depth at Site 723, and relatively low values characterizing the Miocene turbidites on the Owen Ridge (Fig. 10). Two main factors govern these distributions. First, high ammonia levels on the Oman Margin reflect the anaerobic degradation of buried organic matter; at Site 723 this is particularly pronounced as noted above. Second, the turbidites contain very little organic material and therefore little organic nitrogen which is the precursor for pore water ammonia, and they also contain illite which is known to exchange K^+ for NH_4^+ (Müller, 1977). It is probable that uptake of NH_4^+ by illite and mixed-layer clays is responsible for the downward decrease in the NH_4^+ profile seen between 100 and 400 mbsf at the Owen Ridge sites.

In contrast to the high levels of ammonia seen in margin sediments, phosphate concentrations are low (Table 1). We attribute the widespread deficiency to the precipitation of authigenic fluorapatite, which occurs in visible quantities at several margin sites (e.g., Site 723) as brown-to-golden or black aggregates or clasts up to 2 mm in size with a knobby surface texture, and friable to indurated nodules up to 5 cm diameter at Site 726. The latter occurrence was interpreted to represent a lag deposit. The composition of both forms of the phosphorite was confirmed by X-ray diffractometry, which yielded the characteristic spectrum of carbonate fluorapatite (francolite).

THE SULFATE PROBLEM: COMPARISON WITH THE PERU MARGIN

Despite the co-occurrence of high productivity and consequent high settling flux of organic carbon (see Table 2) and dysaerobic bottom waters along much of the Oman Margin, the rate of sulfate depletion in the pore waters is not pronounced when compared to hemipelagic settings elsewhere. To illustrate this contrast, we have compared in Figure 11 the relationship between linear sedimentation rate and the rate of sulfate depletion as a function of depth for the Peru and Oman Margins. The data used in this plot are listed in Table 3. The Peru Margin data are taken from Suess, von Huene, et al. (1988, p. 16). The Oman Margin data are calculated for the five sites listed using the age (0.19 Ma) and depth of first appearance of *Emiliania huxleyi* for the determination of average late Pleistocene sedimentation rates, and the slopes of the sulfate profiles determined from the data in Table 1 using only measurements from the upper 20–50 m at each site. Note that data from Sites 726 (deposition punctuated by hiatuses) and 729 (poor recovery) are not included in the compilation.

It is clear from Figure 11 that a considerable difference exists between the relative rates of sulfate reduction at a given sedimentation rate on the two margins. We suspect that the reason for this contrast lies in the nature of the organic matter which is buried in each region. Organic matter at most of the Peru Margin sites tends to be lipid-rich and has a relatively high mean hydrogen index and a low oxygen index (Suess, von Huene, et al., 1988). These characteristics imply that the organic material is in general well preserved and of marine origin. In contrast, organic matter on the Oman Margin tends to be degraded to a significant degree even before burial. Relatively high C/N ratios typify organic detritus in surface sediments from the area (Wiseman and Bennett, 1940; Shimmield et al., 1990), irrespective of the bottom water oxygen concentration (Calvert and Pedersen, in press). Shimmield et al. (1990) have shown that a strong positive correlation exists between the degree of reworking of the sediments, as indicated by the Cr content (which proxies for the proportion of heavy minerals present) and the degree of degradation as evinced by the C/N ratio. Hydrogen and oxygen index measurements made by pyrolysis during Leg 117 (Prell, Niitsuma, et al., 1989) similarly suggest that the organic matter along the margin is less labile than on the slope off Peru. $\delta^{13}C$ measurements made on the organic fraction at Site 724 (Muzuka et al., this volume) indicate that the organic inventory in the sediments is dominated by marine organic matter, which is consistent with the low or absent input of fluvial (thus, terrestrial) detritus along the margin. Therefore, we do not believe that the apparent refractory nature of the buried carbon compounds is a reflection of a predominance of terrigenous material.

On a broader scale, it is not clear why there should be such a contrast between the nature of the organic matter buried on the Peru and Oman Margins. The particle flux to the deep Western Arabian Sea during the southwest monsoon appears to be dominated by coccolithophorids (Nair et al., 1989). In contrast, diatoms dominate the settling flux on the Peru Margin (Henrichs and Farrington, 1984). The compositions of the bulk sediments underlying both upwelling regimes attest to this contrast: nannofossil-foram ooze (rarely diatomaceous: Shimmield et al., 1990) characterizes much of the Oman Margin, while diatomaceous ooze typifies the deposits on the slope off Peru. It may be that the character of the organic matter delivered to the sediment-water interface, a portion of which is subsequently buried, is sufficiently different on the two margins as to generate the observed diagenetic contrast. The difference clearly warrants further, and detailed, investigation.

CONCLUSIONS

Interstitial water profiles were collected during Leg 117 from a single site on the Indus Fan, three sites on the Owen Ridge, and eight sites on the Oman Margin. Diagenetic reactivity is ob-

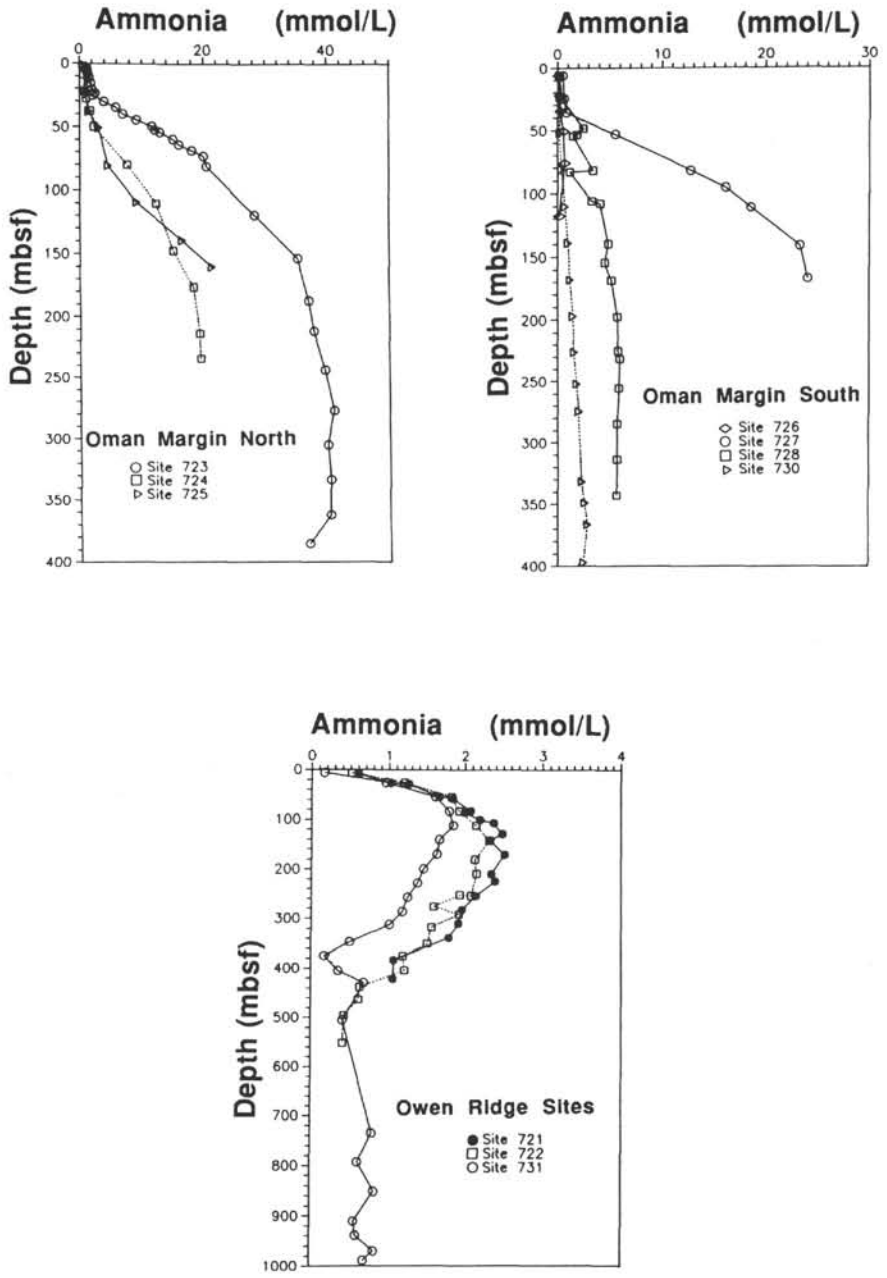

Figure 10. Ammonia profiles in interstitial waters at Owen Ridge and Oman Margin sites, Leg 117.

served to varying degrees at all locations, but is most pronounced on the Oman Margin, where high rates of accumulation of organic matter are characteristic. Extremely high alkalinities at Site 723 reflect quantitative sulfate reduction, and ammonia production during methanogenesis. The co-occurrence of sulfate and enriched calcium at depth along with a chloride deficiency and physical indications of undercompaction suggest that upward migration of a fluid of unusual composition is occurring at this mid-slope location. Widespread magnesium depletions on the margin and the ridge are attributed to the ubiquitous precipitation of dolomite or dolomitization of preexisting calcite. The presence of dolomite stringers at Site 723 is attributed to their formation during episodes when the sedimentation rate was low but productivity was high, possibly during sea level transgressions. Authigenic carbonate fluorapatite is also widespread on the margin. The precipitation of this material can explain the low phosphate concentrations observed in pore waters.

Although sulfate is quantitatively depleted from interstitial solution at depth at most of the drilled sites, the rate of depletion as a function of depth is significantly less than expected, and markedly less than that observed on the Peru Margin where similarly high rates of upwelling and organic carbon accumulation occur. The reason for this contrast is not clear but it may reflect differences in the degree of reworking of organic matter prior to burial on each of the two margins, or a generic differ-

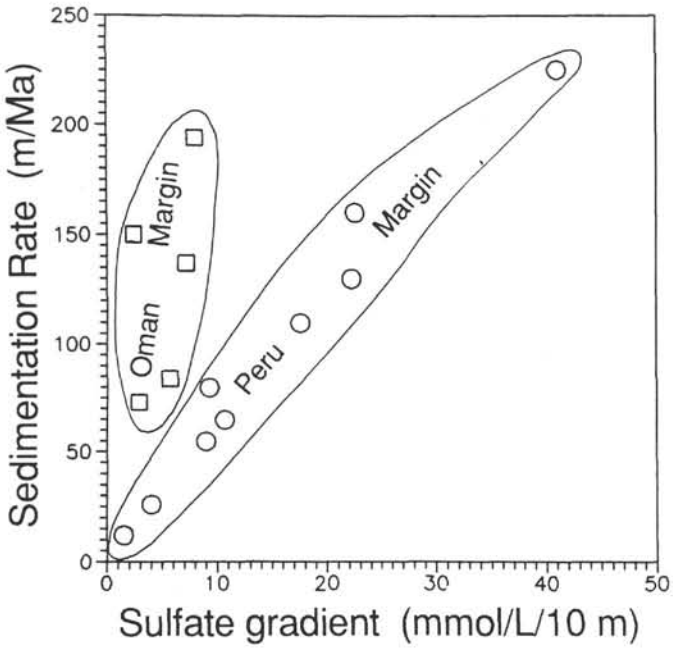

Figure 11. Sedimentation rates plotted against rates of sulfate depletion at Oman Margin and Peru Margin sites.

Table 3. Rates of sulfate depletion as a function of depth at Oman and Peru Margin sites.

Site	Sed. rate (m Ma^{-1})	ΔSO_4^{2-} (mmol L^{-1} per 10 m)
Oman Margin		
723	194	8
724	84	5.7
725	150	2.4
727	137	7.2
728	73	2.9
Peru Margin		
679	12	1.5
680	55	9
681	80	9.3
682	26	4
683	110	17.6
684	?	14.7
685	130	22.3
686	160	22.6
687	65	10.7
688	150–300	41

Note: Derivation of the data is described in the text.

ence in the nature of the organic matter which is produced in the upwelling regimes in the two areas. This highly interesting contrast begs further investigation.

ACKNOWLEDGMENTS

We are very grateful to the shipboard technical staff during Leg 117 for their assistance with sampling and analysis. In particular, Katie Sigler-Tauxe, John Weisbruch and Bettina Domeyer freely offered advice and direction. Their skills and hard work in the laboratory are highly appreciated. We are also grateful for the discussions, sometimes spirited, held on board with our scientific colleagues, and in particular with the organic geochemists, Kay Emeis and Lo ten Haven. B. J. Presley and M. Hartmann, and Kay Emeis offered constructive comments on the manuscript.

TFP and GBS respectively thank the Natural Sciences and Engineering Research Council of Canada and the Natural Environment Research Council (U.K.) for financial support.

REFERENCES

Baker, P. A., and Burns, S. J., 1985. Occurrence and formation of dolomite in organic-rich continental margin sediments. *AAPG Bull.*, 69: 1917–1930.

Baker, P. A., and Kastner, M., 1981. Constraints on the formation of sedimentary dolomites. *Science,* 213:214–216.

Bischoff, J. L., Greer, R. E., and Luistro, A. O., 1970. Composition of interstitial waters of marine sediments: temperature of squeezing effect. *Science,* 167:1245–1246.

Calvert, S. E., and Pedersen, T. F., in press. Organic carbon accumulation and preservation in marine sediments: How important is anoxia? *In* Whelan, J. K., and Farrington, J. W. (Eds.), *Productivity, Accumulation and Preservation of Organic Matter in Recent and Ancient Sediments:* New York (Columbia Univ. Press).

Fanning, K. A., and Pilson, M.E.Q., 1971. Interstitial silica and pH in marine sediment: some effects of sampling procedures. *Science,* 173: 1225–1231.

Gieskes, J.M., and Peretsman, G., 1986. Water chemistry procedures aboard *JOIDES Resolution*—some comments. *ODP Tech. Note,* 5.

Gieskes, J. M., and Rogers, W. C., 1973. Alkalinity determination in interstitial waters of marine sediments. *J. Sediment. Petrol.,* 43:272–277.

Haq, B. U., Hardenbol, J., and Vail, P. R., 1987. Chronology of fluctuating sea levels since the Triassic. *Science,* 235:1156–1167.

Henrichs, S. M., and Farrington, J. W., 1984. Peru upwelling region sediments near 15°S. 1: Remineralization and accumulation of organic matter. *Limnol. Oceanogr.,* 29:1–19.

Hurd, D. C., and Theyer, F., 1975. Changes in the physical and chemical propoerites of biogenic silica from the Central Equatorial Pacific. I: Solubility, specific surface area, and solution rate constants of acid-cleaned samples. *In* Gibb, T.R.P., Jr. (Ed.), *Analytical Methods in Oceanography.* Am. Chem. Soc., Advances in Chemistry Series, 211–239.

Mangelsdorf, P. C., Wilson, T.R.S., and Daniel, E., 1969. Potassium enrichments in interstitial waters of recent marine sediments. *Science,* 165:171–174.

McDuff, R. E., 1985. The chemistry of interstitial waters, Deep Sea Drilling Project, Leg 86. *In* Heath, G. R., Burckle, L. H., et al., *Init. Repts. DSDP,* 86: Washington (U.S. Govt. Printing Office), 675–687.

McDuff, R. E., and Gieskes, J. M., 1976. Calcium and magnesium profiles in DSDP interstitial waters: diffusion or reaction? *Earth Planet Sci. Lett.,* 33:1–10.

Müller, P. J., 1977. C/N ratios in Pacific deep-sea sediments: effect of inorganic ammonium and organic nitrogen compounds sorbed by clays. *Geochim Cosmochim. Acta,* 41:765–771.

Müller, P. J., and Suess, E., 1979. Productivity, sedimentation rate, and sedimentary organic matter in the oceans. I. Organic carbon preservation. *Deep-Sea Res. Part A,* 26:1347–1362.

Murray, J. W., Emerson, S., and Jahnke, R., 1980. Carbonate saturation and the effect of pressure on the alkalinity of interstitial waters from the Guatemala Basin. *Geochim. Cosmochim. Acta,* 44:963–972.

Nair, R. R., Ittekkot, V., Manganini, S. J., Ramaswamy, V., Haake, B., Degens, E. T., Desai, B. N., and Honjo, S., 1989. Increased particle flux to the deep ocean related to monsoons. *Nature,* 338:749–751.

Prell, W. L., and Niitsuma, N., et al., 1989. *Proc. ODP. Init. Repts,* 117: College Station, TX (Ocean Drilling Program).

Quasim, S. Z., 1982. Oceanography of the northern Arabian Sea. *Deep-Sea Res. Part A,* 29:1041–1068.

Sayles, F. L., and Manheim, F. T., 1975. Interstitial solutions and diagenesis in deeply buried marine sediments: results from the Deep Sea Drilling Project. *Geochim. Cosmochim. Acta,* 39:103–128.

Shimmield, G. B., and Price, N. B., 1984. Recent dolomite formation in hemipelagic sediments off Baja California, Mexico. *In* Garrison, R. E., Kastner, M., and Zenger, D. H. (Eds.), *Dolomites of the*

Monterey Formation and Other Organic-Rich Units: Pacific Section S.E.P.M., 41:5–18.

Shimmield, G. B., Price, N. B., and Pedersen, T. F., 1990. The influence of hydrography, bathymetry, and productivity on sediment type and composition from the Oman margin and the northwest Arabian Sea. *In* Robertson, A.H.F., Searle, M. P., and Ries, A. C. (Eds.), *The Geology and Tectonics of the Oman Region:* Geol. Soc. Am. Spec. Publ., 49:759–769.

Sholkovitz, E. R., 1973. Interstitial water chemistry of the Santa Barbara Basin sediments. *Geochim. Cosmochim Acta,* 37:2043–2073.

Suess, E., von Huene, R., et al., 1988. *Proc. ODP. Init. Repts.*, 112: College Station, TX (Ocean Drilling Program).

Wiseman, J.D.H., and Bennett, H., 1940. The distribution of organic carbon and nitrogen in the sediments from the Arabian Sea. *Rep. John Murray Exped.,* 3:193–221.

Wyrtki, K., 1971. *Oceanographic Atlas of the International Ocean Expedition:* Washington (Nat. Sci. Found.).

Date of initial receipt: 2 October 1989
Date of acceptance: 8 May 1990
Ms 117B-152